

Band Structures of ^{182}Os Studied by GCM based on 3D-CHFB

Takatoshi Horibata^{a,c} *, Makito Oi^{b,c}, Naoki Onishi^{b,c} and Ahmad Ansari^{b,d}

^a*Department of Information System Engineering, Aomori University, Aomori-city, Aomori 030-0943, Japan*

^b*Institute of Physics, College of Arts and Sciences, University of Tokyo, Komaba, Meguro-ku, Tokyo 153-8902, Japan*

^c*Cyclotron Laboratory, Institute of Physical and Chemical Research(RIKEN), Hirosawa 2-1, Wako-city, Saitama 351-0198, Japan*

^d*Institute of Physics, Doordarshan Marg, Bhubaneswar 751005, India*

(February 9, 2008)

Band structure properties of ^{182}Os are investigated through a particle number and angular momentum constrained generator coordinate(GCM) calculation based on self-consistent three-dimensional cranking solutions. From the analysis of the wave function of the lowest GCM solution, we confirm that this nucleus shows a tilted rotational motion in its yrast states, at least with the present set of force parameters of the pairing-plus-quadrupole interaction Hamiltonian. A close examination of behavior of other GCM solutions reveals a sign of a possible occurrence of multi-band crossing in the nucleus. Furthermore, in the course of calculations, we have also found a new potential curve along the prime meridian on the globe of the $J = 18\hbar$ sphere. Along this new solution the characters of proton and neutron gap parameters get interchanged. Namely, Δ_p almost vanishes while Δ_n grows to a finite value close to the one corresponding to the principal axis rotation(PAR). A state in the new solution curve at the PAR point turns out to have almost the same characteristic features of an yrare s -band state which gets located just above the g -band in our calculation. This fact suggests a new type of seesaw vibrational mode of the proton and the neutron pairing, occurring through a wobbling motion. The mode is considered to bridge the g -band states and the s -band states in the backbending region.

Keywords: generator coordinate method, cranked HFB, tilted axis rotation, band crossing

PACS numbers: 21.60.-n, 21.60.Ev, 27.70.+q

I. INTRODUCTION

A limitation of a framework of the nuclear mean field approach whose validity is supported by the success of the idea of an independent particle motion has become one of the central matter of concern in recent years in nuclear physics. When we describe, for instance, high- K states in a γ -soft nucleus or a large amplitude collective motion(LACM), such as a fission or a process which leads to break up into fragmentation, which has recently attracted much attention through the molecular dynamics analysis, an assumption of stiffness against deformation is no longer valid. Furthermore, in the nuclear halo or in a skin structure only a small number of nucleons come into play in the region, and therefore the notion of a formation of a stable mean field will hardly be acceptable in such exotic situations. For the description of these new topics one thinks of the two representative theories: the time dependent Hartree-Fock(TDHF) and the generator coordinate method [1]. They demonstrate their full ability in description of such situations. Particularly, the GCM is fully quantum mechanical and it can be applied to wide range of problems. Especially in the situations where several potential minima come into play in the motion. For instance, LACM; in the situations of including a super deformation or a hyper deformation, it will be one of the promising methods because it expresses states as a superposition of many different product wave

functions and can describe tunneling effects among the potential minima. The basic idea of this method which goes beyond the conventional mean field theory, may well continue as one of the reliable frameworks in the coming century.

Since the nuclei in the region of osmium and tungsten generally exhibit softness against the γ -deformation [2] they provide a nice testing ground for an approach which goes beyond the mean field theory. We have been carrying out a systematic calculation based on a self-consistent three-dimensional cranked Hartree-Fock-Bogoliubov(3D-CHFB) theory in ^{182}Os and have found a solution which suggests the existence of a tilted axis rotating(TAR) state [3]. The resulting potential curve along the prime meridian on the globe of $J = 18\hbar$ sphere has two TAR minima which locate symmetrically with respect to an equatorial plane. Thus the GCM calculation by taking into account the north and the south latitude as a generator coordinate to describe excited states is a highly interesting problem.

Our previous attempts based on the GCM calculations, however, suffer from some difficulties [4]. The first point was that in our calculation somewhat large energy splittings among the GCM solutions were obtained. Since we wish that our GCM solutions should correspond to the observed level spacings above the yrast states, the calculated energy spacings among these solutions should stay within the range of $10\text{keV} \sim 100\text{keV}$. The second difficulty

in our calculation was that we hardly obtained any stable GCM solutions in the high angular momentum region.

One of the problems in our approach is that we lose much information concerning the high frequency part of wave functions when we solve the GCM equation. Because in solving the GCM equation we have discarded the eigenstates of the norm overlap kernel whose eigenvalues are negligibly small. These states bring serious numerical errors when the equation is numerically solved [12]. Therefore, they are considered to be unfavorable. The other possible problem is that although the TAR potential spread non-locally over a surface of a globe with a constant angular momentum, we restricted the Hill-Wheeler integration to one-dimensional coordinate, that is we restricted the calculation only along the prime meridian. These drawbacks of our approach will be remedied by introducing the the angular momentum projection techniques [6] and the two-dimensional Hill-Wheeler integration [5]. Since the programs for carrying out such calculations will become a project of inevitably exhaustive investigation, more basic study about the characteristic features of GCM solutions at this moment must be helpful.

Generally, in the process of solving the GCM equation the expectation values of the angular momentum and the particle number may get shifted from the values of the CHFB constraints. For instance, the amplitudes of lower angular momentum components present in the cranking wave function will increase their probabilities in such a way to reduce the total energy of the system. To keep the correct configuration of wave functions we restrict the expectation values of the angular momentum and particle number to their given values during the process of solving the GCM equation. Applying the constrained GCM method [7] to the TAR potential curve to obtain the improved solutions is one of the main motivations of the present work.

By solving the constrained GCM equations in case of ^{182}Os at $J = 18\hbar$ we have found that the wave functions have symmetric or anti-symmetric properties with respect to the generator coordinate. This means that the broken symmetry of signature in TAR wave function has been recovered through the GCM procedure. Analyzing the wave function we have found that this nucleus must be a tilted-rotor in the present parameter set. Furthermore, we have found the existence of the PAR components in the excited GCM solutions. This result is very interesting because we have solved the GCM equations based on the TAR potential which shows the minimum points located at a distance from the principal axis. This fact exhibits a sign of existence of a different band structure in the GCM solutions at $J = 18\hbar$ state. We will discuss a possibility of multi-band crossing in this nucleus. Some preliminary results of our study are already presented in a short article [8].

In the next section 2 a brief sketch of the formalism

is presented. Results and discussions are presented in section 3. Finally section 4 contains a brief summary and conclusions of the present investigations.

II. CALCULATIONAL METHOD

In this section we describe briefly the framework of our model. Details of the calculational methods for the 3D-CHFB and for the Hill-Wheeler equation are presented in our previous works [4,9,10].

The model Hamiltonian used in the present study is the pairing plus Q - Q force given by,

$$\hat{H} = \sum_i \epsilon_i c_i^\dagger c_i - \frac{1}{2} \kappa \sum_{\mu=-2}^2 (-)^{\mu} \hat{Q}_{-\mu} \hat{Q}_{\mu} - \sum_{\tau=p,n} g_{\tau} \hat{P}_{\tau}^\dagger \hat{P}_{\tau}, \quad (1)$$

where ϵ_i represents the single particle energies and c_i^\dagger and c_i are the creation and the annihilation operators for particle states $|i\rangle$. Conditions $c_i |0\rangle = 0$ hold for all i , and $|0\rangle$ stands for the true vacuum. The parameters κ and g_{τ} are the corresponding interaction strengths. The quadrupole operator is defined,

$$\hat{Q}_{\mu} = \sum_{ij} \langle i | r^2 Y_{2\mu} | j \rangle c_i^\dagger c_j, \quad (2)$$

as well as the pairing,

$$\hat{P}_{\tau}^\dagger = \sum_{i_{\tau} > 0} c_{i_{\tau}}^\dagger c_{i_{\tau}}. \quad (3)$$

This Hamiltonian is very simple for calculation but still effective in describing essential features of the nuclear deformation and the pairing correlation.

In the present work the Hill-Wheeler equation is modified to include the constraint on the expectation values of the angular momentum and the particle number operators. As usual, first the norm overlap kernel is diagonalized,

$$\int n(\psi, \psi') u_k(\psi') d\psi' = \nu_k u_k(\psi), \quad (4)$$

where $n(\psi, \psi')$ is Hermitian matrix defined as,

$$n(\psi, \psi') = \langle \Phi(\psi) | \Phi(\psi') \rangle. \quad (5)$$

The wave function $\Phi(\psi)$ is the solution of the following 3D-CHFB equation with eight constraints,

$$\delta \langle \Phi | \left[\hat{H} - \sum_{k=1}^3 \left(\mu_k \hat{j}_k + \xi_k \hat{B}_k \right) - \sum_{\tau=p,n} \lambda_{\tau} \hat{N}_{\tau} \right] | \Phi \rangle = 0, \quad (6)$$

where μ_k , ξ_k and λ_τ are the Lagrange multipliers which are adjusted to satisfy the following constraints,

$$\langle \Phi | \hat{J}_k | \Phi \rangle = j_k \quad (k = 1, 2, 3), \quad (7)$$

$$\langle \Phi | \hat{N}_\tau | \Phi \rangle = n_\tau \quad (\tau = p, n), \quad (8)$$

and

$$\langle \Phi | \hat{B}_k | \Phi \rangle = 0 \quad (k = 1, 2, 3), \quad (9)$$

where \hat{B}_k 's express three off-diagonal elements of the mass-quadrupole tensor in Cartesian-coordinate representation,

$$\hat{B}_k = \frac{1}{2}(\hat{Q}_{ij} + \hat{Q}_{ji}) \quad (ijk; \text{cyclic}). \quad (10)$$

We know from our previous study that a calculation along the prime meridian always gives lower energy when compared with the calculation performed on the whole surface of the globe [9]. Therefore, in the present study we restrict the generator coordinate only to the latitude ψ along the prime meridian. Thereby the CHFB equations become now only two-dimensional. The angle ψ is measured with respect to the x -axis so that $\hat{J}_1 = \hat{J} \cos \psi$, $\hat{J}_2 = 0$ and $\hat{J}_3 = \hat{J} \sin \psi$. This also helps us not to face any problem in choosing the phase in the square root which will appear in the calculation of eq.(5) [11]. By utilizing the eigenfunctions $u_k(\psi)$ of the overlap kernel, eq.(4), we can construct the orthogonal sets which are called the natural states [12],

$$|k\rangle = \frac{1}{\sqrt{\nu_k}} \int u_k(\psi) | \Phi(\psi) \rangle d\psi. \quad (11)$$

Generally, in the process of solving the GCM equation the expectation values of angular momentum and the particle numbers will somewhat get shifted from the values of the CHFB constraints. To keep the appropriate wave functions we restrict the expectation values of the scalar of squared angular momentum vector \mathbf{J}^2 and particle numbers to their correct values during the process of solving the GCM equations. Therefore we solve the following constrained Hill-Wheeler equation,

$$\sum_{k'} \left[H_{k,k'} - \lambda_\tau^{(\alpha)} N_{k,k'}^\tau - \mu^{(\alpha)} \mathbf{J}_{k,k'}^2 \right] g_{k'}^{(\alpha)} = E^{(\alpha)} g_k^{(\alpha)}. \quad (12)$$

The Lagrange multipliers $\lambda_\tau^{(\alpha)}$ and $\mu^{(\alpha)}$ in eq.(12) control the expectation values of particle numbers and the square of angular momentum in the GCM wave functions and are different from those appearing in eq.(6). The superscript “ α ” indicates the index of the eigenstates. The matrices $H_{k,k'}$, $N_{k,k'}^\tau$ and $\mathbf{J}_{k,k'}^2$ are given as follows,

$$H_{k,k'} = \int d\psi d\psi' \frac{u_k^*(\psi)}{\sqrt{\nu_k}} \langle \Phi(\psi) | \hat{H} | \Phi(\psi') \rangle \frac{u_{k'}(\psi')}{\sqrt{\nu_{k'}}}, \quad (13)$$

$$N_{k,k'}^\tau = \int d\psi d\psi' \frac{u_k^*(\psi)}{\sqrt{\nu_k}} \langle \Phi(\psi) | \hat{N}_\tau | \Phi(\psi') \rangle \frac{u_{k'}(\psi')}{\sqrt{\nu_{k'}}}, \quad (14)$$

and

$$\mathbf{J}_{k,k'}^2 = \int d\psi d\psi' \frac{u_k^*(\psi)}{\sqrt{\nu_k}} \langle \Phi(\psi) | \hat{J}^2 | \Phi(\psi') \rangle \frac{u_{k'}(\psi')}{\sqrt{\nu_{k'}}}. \quad (15)$$

Detailed expressions for the matrix elements appearing in the integration are given in Ref. [4]. The eigenstates of our GCM equation are given by,

$$| \Psi_\alpha \rangle = \sum_{k, \nu_k \neq 0} g_k^{(\alpha)} | k \rangle, \quad (16)$$

where $g_k^{(\alpha)}$ are obtained as solutions of eq.(12). From eq.(11) we find the corresponding weight function,

$$f^{(\alpha)}(\psi) = \sum_{k, \nu_k \neq 0} g_k^{(\alpha)} u_k(\psi). \quad (17)$$

Then, finally the physical quantities are calculated using the matrix elements in eq.(13-15) and the wave function $g_k^{(\alpha)}$ as follows,

$$\begin{pmatrix} H^{(\alpha)} \\ N_\tau^{(\alpha)} \\ J^{2(\alpha)} \end{pmatrix} = \sum_{k, k'} g_k^{*(\alpha)} \begin{pmatrix} H_{k,k'} \\ N_{k,k'}^\tau \\ \mathbf{J}_{k,k'}^2 \end{pmatrix} g_{k'}^{(\alpha)}. \quad (18)$$

III. NUMERICAL RESULTS AND DISCUSSIONS

A. Solution of 3D-CHFB equations

Recently a systematic calculation based on the 3D-CHFB theory revealed the possible existence of a tilted axis rotating potential in ^{182}Os nucleus [3,9]. In our previous calculations, however, the force parameters were chosen so as to reproduce just the overall features of low-angular momentum states of nuclei in this mass region. The observed first backbending in $A \sim 180$ region is expected to be due to $i_{13/2}$ neutron alignments, whereas in our earlier calculation protons were playing the role. The reason was attributed to our slightly too strong Q·Q force parameter and also to rather strong pairing interaction for neutrons. In the present calculation we reduced the Q·Q force parameter and the strength of neutron pairing interaction so as to make rotation alignment of neutron occur in the PAR states, which is considered to be yrast

in ^{182}Os . Our new force parameters are chosen so as to give as $\beta = 0.280$, $\Delta_p = 1.040\text{MeV}$ and $\Delta_n = 0.925\text{MeV}$ in the ground state. Moreover, we have attained considerable high precisional calculation this time. We have increased the number of iteration to achieve better convergence when solving by the steepest descent method. We have fixed an increment of angular momentum as $\Delta J = 0.1\hbar$ in the calculation along the yrast line up to $J = 30\hbar$ and set the maximum iteration for convergence as 300 times and the minimum iteration as 50 times for each step. In our previous calculation, those iteration times were taken as 120 and 30, respectively. The size of the model space and the single particle energies ϵ_i in the Hamiltonian are not changed from our previous study. They are shown in Table 1 together with quantum numbers such as isospin, radial node number, orbital angular momentum and total angular momentum [13].

In a similar manner as the previous papers, we obtained PAR solutions by cranking up along x -axis perpendicular to the symmetry axis of the non-rotating state and also by cranking down along the axis. The two bands cross at $J \sim 20\hbar$ in the present case. At the crossing point in the g -band the size of proton gap parameter is $\Delta_p = 0.87\text{MeV}$ and the neutron gap parameter almost vanishes. The characteristic features of the yrast line are indicated in Fig.1.

Model space and single particle energies

proton	
orbits	energy (MeV)
$1f_{7/2}$	8.06435
$0i_{13/2}$	7.55675
$0h_{9/2}$	7.23480
$2s_{1/2}$	3.87120
$1d_{3/2}$	3.59468
$0h_{11/2}$	2.16538
$1d_{5/2}$	1.29040
$0g_{7/2}$	0.64520
$0g_{9/2}$	-3.50251

neutron	
orbits	energy (MeV)
$0i_{11/2}$	7.55740
$1g_{9/2}$	6.74629
$2p_{1/2}$	4.40579
$1f_{5/2}$	3.39191
$2p_{3/2}$	3.02322
$0i_{13/2}$	1.56626
$0h_{9/2}$	0.82954
$1f_{7/2}$	0.16591
$0h_{11/2}$	-4.23988

Table 1: Model space and the single particle energies in the present calculation. In the space 36 valence particles and 40 core particles are taken for the proton and also

36 valence particles and 70 core particles are considered for the neutron.

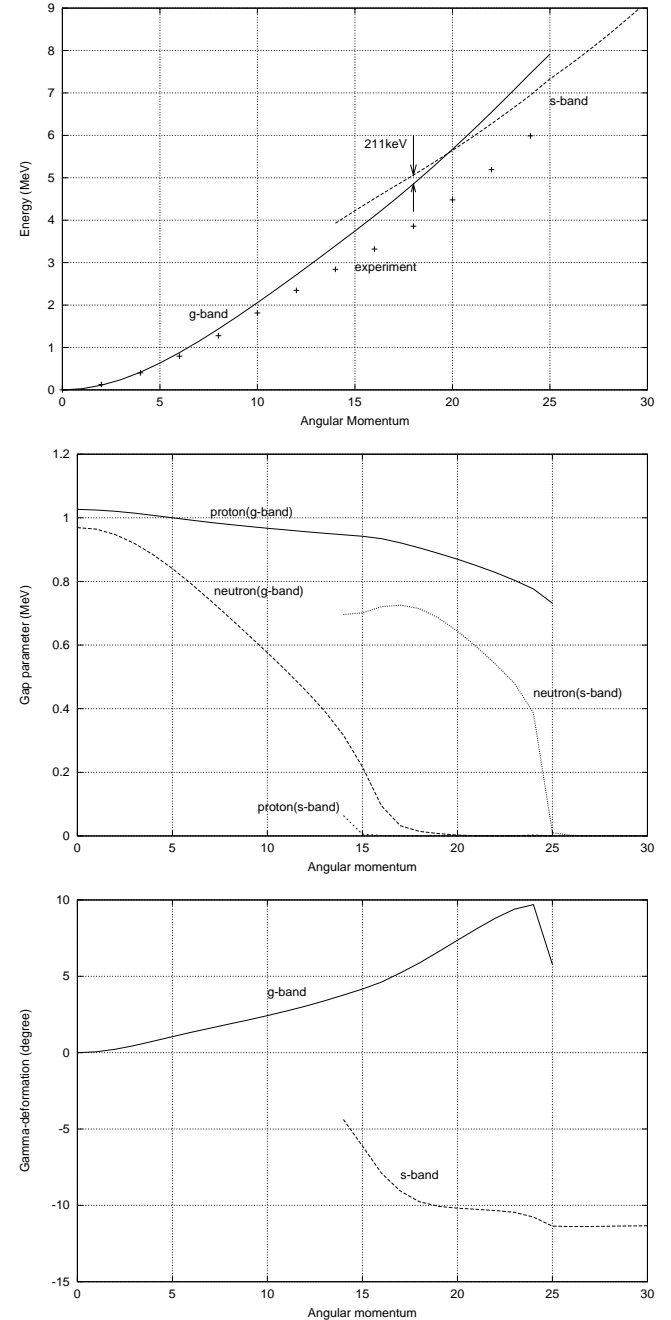


FIG. 1. Fig.1a shows the behavior of energy curves of the g -band and the s -band as well as the experimental value. The two bands cross at $J \sim 20\hbar$ in our calculation. The energy value 211keV indicated in the figure shows the energy difference between the $J = 18\hbar$ yrast state and the yrast state. Fig.1b shows the behavior of the gap parameters for each band. The change of γ -deformation is indicated in Fig.1c.

Fig.1a shows the behavior of energy curves of the g -band and the s -band as well as the experimental value

taken from Ref. [2]. In our previous calculation [9] both bands cross at $J = 14\hbar$ due to the proton alignment. In the present case, after the band crossing at $J = 20\hbar$ the g -band continues up to $J = 25\hbar$ state. We can not obtain any g -band components above this state and after the intensive iteration processes the CHFB solution finally converges to a next state which belongs to the s -band. In the same manner, the s -band obtained by cranking down calculation continues down to $J = 14\hbar$ state. When decreasing the angular momentum by a unit $0.1\hbar$ from this state the solution converges to a new state in the g -band after many iteration processes. In Fig.1b we show the behavior of the gap parameters. The strength of the neutron gap parameter both in the g -band and the s -band are much reduced when they are compared with our previous calculation [9]. In the present calculation, the proton gap parameter almost keeps its value until the end of the g -band. The change of γ -deformation is indicated in Fig.1c. The γ -deformation changes drastically at the band crossing point. The value in the g -band is $\gamma_g = 7.36^\circ$ and in the s -band is $\gamma_s = -10.19^\circ$ at the point.

We tilted rotating axis along the prime meridian, which intersects with z - and x -axis on the sphere of $J = 18\hbar$. As in our previous calculation, here too the existence of a stable TAR state is confirmed in the region of $\psi = 20^\circ \sim 30^\circ$ as shown in Fig.2a.

The TAR minimum takes place at $\psi = 24^\circ$, and its depth is $V_{TAR} = -0.166$ MeV. We can find an occurrence of phase transition between the PAR and the TAR point at about $\psi = 10^\circ$. Starting from the PAR the potential curve ends at this point with its energy $V_{first} = 0.189$ MeV. After this point, a new potential curve with different configuration appears which continues up to $\psi = 42^\circ$. In the region between $\psi = 10^\circ$ and $\psi = 42^\circ$, in which the TAR appears, the proton gap parameter almost vanishes and the neutron gap parameter recovers its original strength of the ground state value as shown in Fig.2b. This fact implies that the TAR is generated due to a collapse of the proton gap parameter in our calculation. Thus the phase transition is considered to be caused by a crossing of a band with $\Delta_n = 0$ and $\Delta_p \neq 0$ to an another band with $\Delta_n \neq 0$ and $\Delta_p = 0$.

We encounter the next phase transition point at 43° with $V_{second} = 0.470$ MeV. At this point the configuration of wave function also changes drastically. That is, the proton gap parameter recovers its strength and oppositely the neutron gap parameter reduces its value to about 70% of the value at the TAR region as shown in Fig.2b. In the region between $\psi = 44^\circ$ and $\psi = 52^\circ$ both the proton and the neutron gap parameters take about $\Delta_p \sim \Delta_n \sim 0.5$ MeV. Calculation above this region, where we did not explore in our previous GCM study, the potential curve shows relatively smooth behavior and it goes down into negative value at the north pole. The energy value at the point is $V_{n-pole} = -0.167$ MeV. This means that the states around the north pole are

lower in energy compared with the PAR state. The wave function of this state consists of the positive parity $i_{13/2}$ neutron which align their angular momenta to the symmetry axis and contribute to $K = 8$ band state. At this moment, we do not have any experimental evidences for the TAR minimum or the existence of energetically lower states near the north pole.

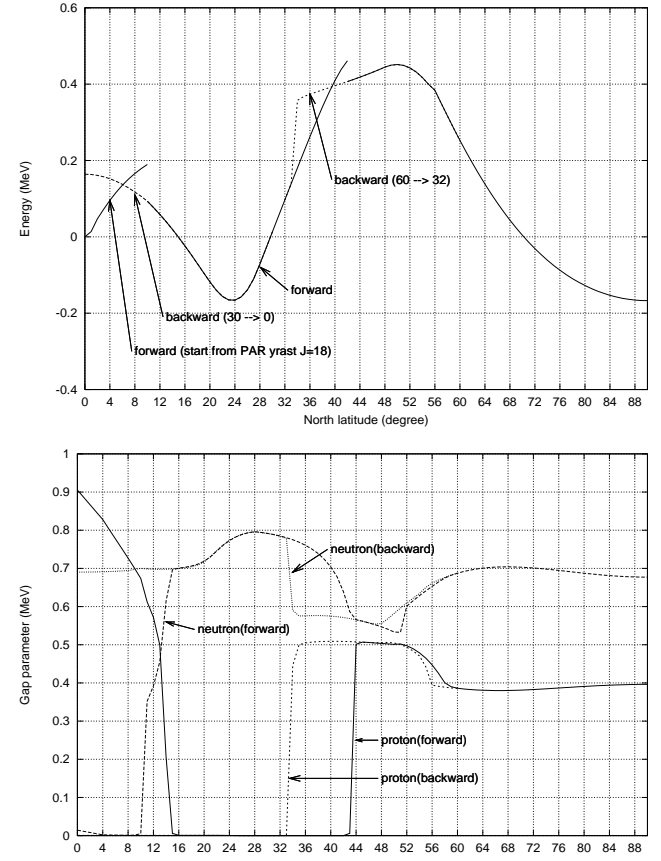


FIG. 2. Fig.2a shows the energy curves along the prime meridian on the globe of $J = 18\hbar$ sphere of ^{182}Os . The solid curves (indicated “forward”) are obtained by increasing the north latitude angle starting from $\psi = 0^\circ$ up to $\psi = 90^\circ$. The two phase transitions are observed at $\psi = 10^\circ$ and $\psi = 42^\circ$. The two dashed curves show the another 3D-CHFB solutions (indicated “backward”) which are obtained by decreasing the angle. Along this new solutions the characters of the proton and the neutron gap parameters mutually get interchanged as seen in Fig.2b. All the energy curves are mirror symmetric with respect to an equatorial plane of the globe. Fig.2b shows behavior of the pairing gap parameters for the proton and the neutron along the curves indicated in Fig.2a. We can see that the TAR potential is caused by a sudden decrease of proton gap parameter and the simultaneous sudden restoration of the neutron gap parameter. Near the PAR point the proton gap parameter Δ_p almost vanishes and the neutron gap parameter Δ_n recovers its value.

The GCM study based on this full potential curve will certainly give some clues to understand the new dynamics

characteristic in this mass region. Unfortunately, our previous calculation were restricted to a region up to the second phase transition point [4].

On the other hand, we show in Fig.2a the existence of another 3D-CHFB solutions along the prime meridian in this nucleus [14]. The first solutions have been obtained by a calculation starting from the point $\psi = 30^\circ$ back to the point $\psi = 0^\circ$. The next solutions starting from the point $\psi = 62^\circ$ back to the point $\psi = 32^\circ$. Along this new first solution the characters of proton and neutron gap parameters mutually get interchanged as shown in Fig.2b. Namely, Δ_p almost vanishes while Δ_n grows up to a finite value at the PAR point. Therefore this new solution has an s_p -band character. At the PAR point, the excitation energy and the gap parameters Δ_p and Δ_n of this new solution takes the close value as that of the yrare s -band state at $J = 18\hbar$. The excitation energy of the new solution at the PAR point is $E_{tilt-back} \sim 164$ keV whereas the energy difference between an yrast g -band state and an yrare s -band state at $J = 18\hbar$ is $E_{g-s} \sim 211$ keV in our calculation(see Fig.1a). The energy difference between the states in the excitation energy is about 47keV. At this moment, we think that this difference arises due to still insufficient convergence during our iteration process. If we start a tilting calculation along the prime meridian from the $E = 211$ keV $J = 18\hbar$ yrare state, a resulting potential curve just after the first phase transition point at $\psi = 10^\circ$ (see Fig.2a) appears very close to the original potential curve which is obtained by starting from the yrast $J = 18\hbar$ PAR state. The new state at the PAR point can naturally be considered as a member of an yrare s -band states, but more precise study will be necessary about this point. The value of gap parameters at the PAR point in the new solution are almost the same as that of the corresponding yrare state in the s -band.

In the present calculation the s -band solutions in the PAR calculation continue down to a state with angular momentum $J = 14\hbar$. Along the solution curve starting inversely from the $J = 30\hbar$ the neutron gap parameter gradually increase up to $\Delta_n = 0.76$ MeV at $J = 16\hbar$. The γ -deformation changes drastically between the yrast and the yrare states at $J = 18\hbar$. The value of the yrast state is $\gamma = 5.88^\circ$ and that of the yrare state is $\gamma = -9.77^\circ$. From these results, we can say that a new type of seesaw vibrational mode of the proton and the neutron pairing, occurring through wobbling motion accompanying the large γ -oscillation, can bridge the yrast state in the g -band and the yrare state in the s -band in the back-bending region of ^{182}Os .

B. Solving GCM equations

We have solved the constrained Hill-Wheeler equation eq.(12) for ^{182}Os at $J = 18\hbar$ in which the north and the

south latitude angles are taken as the generator coordinate. The integration has been carried out in the range of $\psi = -90^\circ \sim 90^\circ$. In numerical calculations we replace the integration over the range into a discrete summation with a step of 4° starting from $\psi = -88^\circ$ to 88° in which totally 45 integration points are contained. The size of the step should be chosen carefully. In the GCM calculation, we first diagonalize the overlap kernel to construct a complete orthogonal set of the GCM wave function. If we set the size to smaller than 4° in the calculation, some eigenvalues of the norm overlap kernel turn negative because of an over-completeness of the overlap kernel. In our calculation all eigenvalues of the norm kernel stay positive and the smallest one is in the order of $\sim 10^{-7}$ which stays in the range of numerical error.

In this study we have carried out two types of calculations. The first type of calculation is the numerical solutions without any constraints whose solutions are shown in Fig.3a. The second one is the solutions in which the expectation values of the squared angular momentum and the particle number operators are constrained. The results are shown in Fig.3b. The lowest ten excited states are shown in both the figures. The abscissa of the figures are the number of eigenstates taken into the calculation of eq.(12) which are obtained from a diagonalization of the norm overlap kernel. The eigenstates are taken in the decreasing order of the size of eigenvalues of eq.(4).

In Fig.3a, we can see that the solutions do not show any stable plateau in the whole range of abscissa coordinates. The situation is not improved at all when compared to our previous works. We only find relatively small plateau in the region of lower excitation energies within a range of abscissa coordinate $35 \sim 40$. The lowest two solutions in the region are almost degenerate and the next higher state lies more than 700keV higher in the energy position. In the previous calculation we also obtained relatively large energy splittings among the GCM solutions and we attributed the reason to relatively deep potential of the TAR. The value was $V_{TAR}^{old} = -0.367$ MeV whereas in the present case the value is $V_{TAR} = -0.166$ MeV. The depth is much smaller this time and the value is less than half of the previous one. From this fact, we can consider that only the shallowness of the TAR potential may not be enough to suppress the size of energy splittings among the states.

In Fig.3b, we can find an existence of relatively large and stable plateaus in the whole range of the abscissa coordinate. The energy splittings among the states are in the range of 10keV \sim 100keV. These values are reasonable for an interpretation of any excited states observed in this mass region. At least the lowest seven states consists relatively stable plateau within the range of abscissa coordinate $30 \sim 35$ (here after we refer this region as *regular*). From the present investigation, we understand that the conservation of the square of angular momentum and the particle number can very much increases the stability

of the GCM solutions. Usually a large angular momentum fluctuation is included in the wave function resulting from a cranking model. Since this value is $\Delta J^2 \sim 100\hbar^2$ in our case, we restrict the expectation value of J^2 to $\sim 420\hbar^2$ for studying the $J = 18\hbar$ state. In solving the Hill-Wheeler equation the expectation value of the total angular momentum does not remain constant when increasing the number of states but drifts to lower angular momentum value to reduce the total energy of the system. This situation can be clearly seen in Fig.4a.

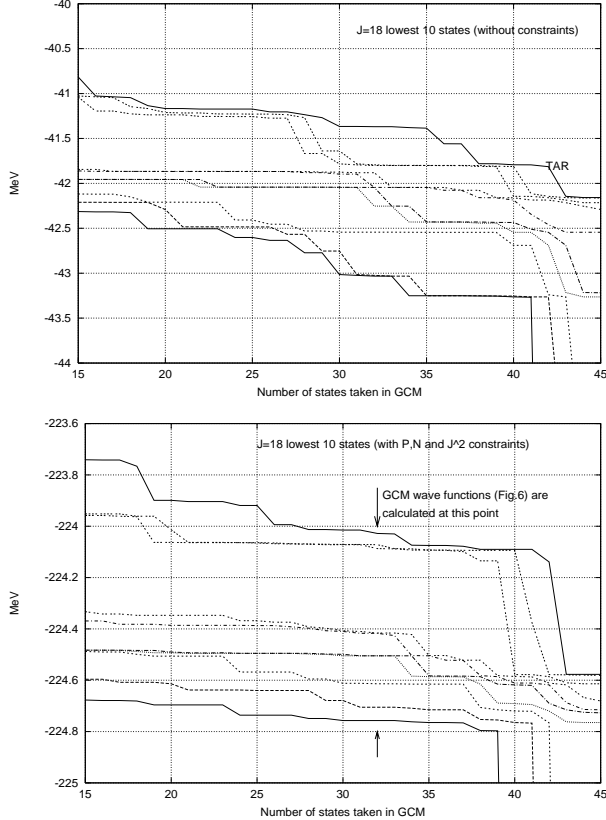


FIG. 3. Several lowest solutions of Hill-Wheeler equations. In the figures the abscissa indicates the number of solutions of eq.(4) considered in solving the equations. Fig.3a shows the solutions without any constraints and Fig.3b indicates the results with particle numbers and the square of angular momentum are constrained(see eq.(12)). Since the wave function in the cranking model suffers from a large angular momentum fluctuation, we took the constrained value of the squared angular momentum value as $J^2 \sim 420\hbar^2$ in the calculation for the $J = 18\hbar$ state. We can see from the figure that the constraints very much contribute to stabilize the GCM solutions. In Fig.3b we indicate the point at which GCM weight functions eq.(17) are calculated(see Fig.6).

The solutions without any constraints do not keep the expectation value of angular momentum. Contamination of lower angular momentum components into our GCM solutions may force the excitation energy of each solution to lower values. This is the main reason for obtaining

the unstable GCM solution when solving with no constraints(Fig.3a). The angular momentum constraint will not be necessary if good angular momentum states are used for the GCM calculation.

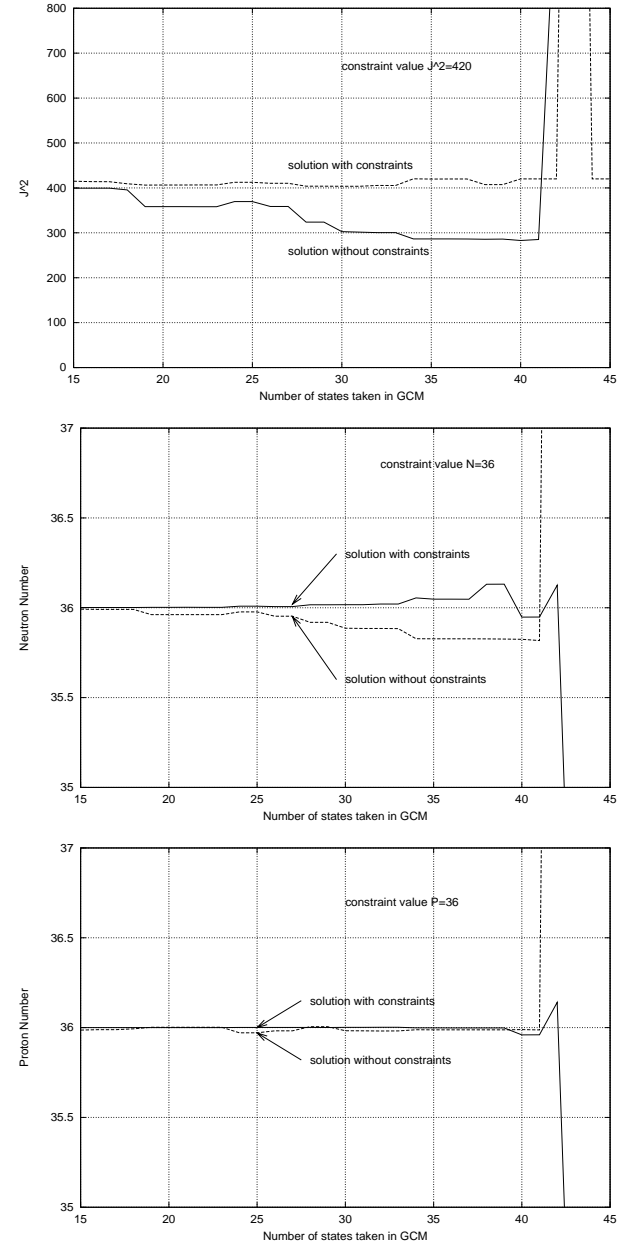


FIG. 4. Comparison of behaviors of the constrained values when solving the Hill-Wheeler equation with and without the constrained terms. Fig.4a indicates the difference of J^2 between the two results. We can see that the decrease of the expectation value of angular momentum in Fig.4a corresponds to the instability of the Hill-Wheeler equation shown in Fig.3a. Fluctuation for the neutron numbers(Fig.4b) and for the proton numbers(Fig.4c) are small in the present study.

In our present study constraints for the particle numbers do not appear to be essential. Following the above discussions, contamination of more particle number com-

ponents in the wave function may lower the total energy of the system. But this tendency may be suppressed by the contamination of lower angular momentum component in the wave function. In our calculation, the fluctuations of particle numbers in the solutions of GCM equations without the constraints are negligibly small, that is, the fluctuation for the neutron is less than 0.56%(Fig.4b) and for the proton the value is almost unchanged(Fig.4c).

Fig.5 shows the probability distribution of the GCM solutions. In the plane the radius of each circle indicates the size of eigenvalue of the equation of norm overlap kernel, eq.(4), which express the probability of each solution. These solutions are taken into account in solving the GCM equations. For instance, the slope of a line for an energy versus J^2 plot(Fig.5a) indicates a value for the chemical potential $\mu^{(1)}$ in the eq.(12). In our calculation this value becomes 6.20×10^{-3} within the *regular* region. From the figure we can see that the solutions are distributed approximately along this line. The most probable GCM states localize around the region $J^2 = 400\hbar^2 \sim 450\hbar^2$ and their energies are about $E' \sim -42\text{MeV}$.

Fig.5b and Fig.5c show the distribution for the GCM solutions in the energy versus particle number plane. We can see the most probable states locate around the value of 36 both for the protons as well as for the neutrons. The chemical potentials in the *regular* region are $\lambda_p^{(1)} = 4.35\text{MeV}$ for the proton and $\lambda_n^{(1)} = 3.66\text{MeV}$ for the neutron. These values are almost constant within the region.

C. Characteristic features of GCM solutions

In Fig.6 we show behavior of the weight functions expressed by eq.(17) for several of the GCM solutions which are obtained from the constrained Hill-Wheeler equation (12). In the calculation, the number of states obtained by eq.(4) which are taken into account in solving eq.(12) are “32”. That point locates within the *regular* region and is indicated in Fig.3b. From Fig.6 we confirm that the GCM solutions have symmetric or anti-symmetric properties with respect to the north and the south latitudes. This means that the broken symmetry of signature in TAR wave function has been recovered through the wobbling motion. All the GCM solutions split into two groups, one is a symmetric group and the other is an anti-symmetric group. In the present case, the first, fourth, fifth, sixth and eighth solutions belong to the symmetric group and the second, third and seventh solutions belong to the anti-symmetric group.

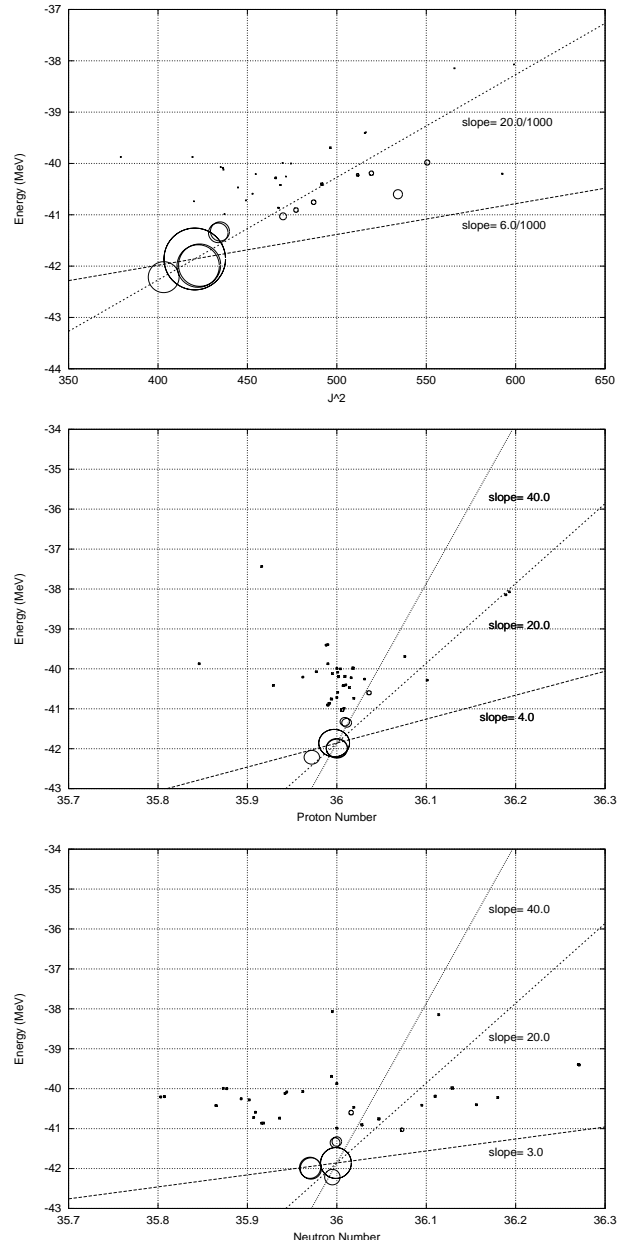


FIG. 5. The probability distribution of the GCM solutions. In the plane the radius of each circle indicates the size of eigenvalue of the equation of norm overlap kernel. The size express the probability of each solution. From the slope of this plot we can reduce the chemical potentials $\mu^{(1)}$, $\lambda_p^{(1)}$ and $\lambda_n^{(1)}$ which appear in eq.(12).

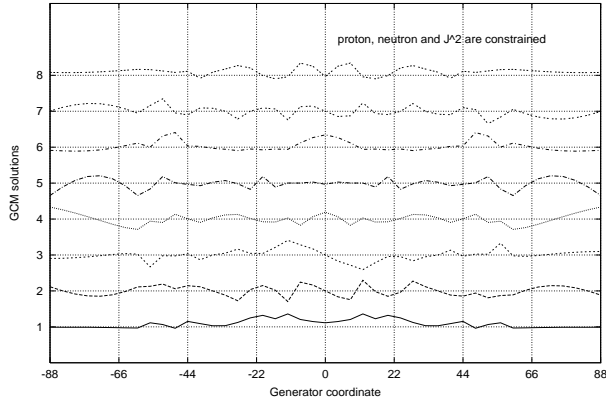


FIG. 6. The weight functions for the several lowest solutions of constrained Hill-Wheeler equation (eq.(12)) at the point indicated in Fig.3b. We can see that the GCM solutions have symmetric or anti-symmetric properties with respect to the north and the south latitudes. This means that the broken symmetry of signature in TAR wave function has been recovered through the wobbling motion.

The lowest solution expresses that this nucleus in the yrast $J = 18\hbar$ state is a tilted-rotor at least for the present set of parameters. The tilt-angle is in the range of $12^\circ \sim 22^\circ$. The most probable angle is $\psi = 12^\circ$. In Fig.2a we show the TAR potential curve which has a minimum point at $\psi = 24^\circ$. There is no guarantee, however, that a nuclear rotational motion will take place about an axis indicated by this angle. In the present approach, only the GCM solutions based on the potential curve can properly describe the characteristic features of nuclear collective motion, such as a tilted axis rotation. This point was not clearly discussed in our previous papers [3,4,9]. Our lowest solution is symmetric with respect to $\psi = 0^\circ$ and is thus characterized as *gerade* state. This solution also exhibits a vestige of a PAR character since it shows a small amplitude at $\psi = 0^\circ$. As already discussed in section 3.1, the PAR state at $J = 18\hbar$ in this nucleus is characterized by the almost vanishing neutron gap parameter and the still surviving proton gap parameter. Therefore we expect that this small PAR component of the state shares a neutron aligned *s*-band character. We call such state as an *s_n*-band state. These PAR characteristic features become remarkable in other solutions obtained at higher excitation energies as discussed below.

The second and the third solutions also show the feature of the tilt states. The most probable tilt-angle for both states is also $\psi = 12^\circ$. The second one, however, shows the tilt characteristic feature also at $\psi = 8^\circ$. These two solutions have no amplitudes at the origin and show anti-symmetric character with respect to $\psi = 0^\circ$. Thus they are grouped into the *ungerade* states.

The fourth and sixth states are the *gerade* states and indicate a nature of the PAR state because they show certain amplitudes at $\psi = 0^\circ$. This result is very interesting because we have solved the GCM equations based on the

TAR potential curve which has the minimum points located at a distance from the principal axis. Since the state with an angular momentum $J = 18\hbar$ is located in the neighborhood of the band crossing point in ^{182}Os , we can naturally expect states with an *s*-band character in the GCM solutions. If above symmetric solutions are the member of an *s_n*-band, understanding of the backbending phenomena in this nucleus becomes quite interesting. P.M.Walker et al. [15] suggested that the backbending is expected to occur due to crossing of a *g*-band with a *t*-band and an *s*-band is not expected to come into play in their study. However, if such a PAR-like solution will come into the lowest state, that is an yrast, in the higher angular momentum region, the situation warrants a somewhat different scenario. The possibility of *s*-band crossing after the *t*-band crossing emerges as one of the backbending mechanisms in this nucleus. Therefore, we have found a sign of multi-band crossing in this nucleus.

The fifth solution also turns out to be a tilt state whose tilt angle is $\psi = 20^\circ$. Since the amplitude of the weight function between these two tilt points is almost negligible, this state may be considered as almost a pure tilted-rotor.

By looking at the higher angle region in Fig.6, we can find that all the lowest seven solutions show certain amplitude in the range of $\psi = 44^\circ \sim 66^\circ$. This result suggests an existence of a high-*K* states ($K = 12 \sim 16$). Further interesting features in the results are that the fourth and the fifth solutions show considerable amplitudes near the region of the north pole. This fact indicates that these solutions also exhibit a character of the deformation aligned state. The total angular momentum $J = 18\hbar$ consists of $J_{n^+} = 8\hbar$ and $J_{p^-} = 10\hbar$. In experiments there are some discussions about the existence of $K = 8^+$ band in osmium [2,16] and tungsten isotopes [15] in connection with an existence of the *t*-band. The interpretation of these deformation aligned states requires more precise analyses theoretically as well as experimentally.

IV. SUMMARY AND CONCLUSIONS

We have carried out the angular momentum and the particle number constrained GCM calculation based on the three-dimensional cranked Hartree-Fock-Bogoliubov approach. Compared to our previous work we have refined the force parameters carefully so as to reproduce the characteristic features of the yrast states of the mass region. With our new set of force parameters the neutron gap parameter Δ_n almost vanishes whereas the proton gap parameter Δ_p still survives with the size of the ground state one at $J = 18\hbar$. In our calculation the band crossing occurs at $J = 20\hbar$. After choosing the force parameter set we have performed the 3D-CHFB calculation along the prime meridian on the globe of $J = 18\hbar$

sphere. We know from our previous study that a calculation along the prime meridian always gives lower energy when compared with the calculation performed on the whole surface of the globe. Like the previous calculation, we have confirmed the existence of a stable TAR potential curve this time also. The TAR curve appears at $\psi = 24^\circ$. Furthermore, here we have found a negative potential curve near the north pole. We have performed the GCM calculation based on this new potential curve and discussed the band structure properties of ^{182}Os . We summarize the present work by stressing following three points.

First point is that by including the constrained terms in the Hill-Wheeler equation the stability of the solutions is much increased and we can recognize in the GCM solutions the appearance of the wide range of plateaus even in such a high angular momentum region as $J = 18\hbar$. This was not the situation in our previous paper [4]. The reason is that we can suppress a drift of the mean value of the square of angular momentum value by the constrained term in the Hill-Wheeler equation and prevent a contamination by the lower angular momentum components present in the cranking wave function.

Second point is that from the symmetry property of the lowest GCM solution we can expect that this nucleus should be a tilted-rotor at $J = 18\hbar$ yrast state. The tilt angle is about $\psi = 12^\circ$. As mentioned in section 3.3 the TAR potential curve will not be a necessary condition for an occurrence of the tilted axis rotation. In our approach only the GCM solutions properly predict the characteristic features of exotic collective motions. In the fourth and the sixth solutions we have found an s -band character in the PAR region. We have found a sign of multi-band mixing in this nucleus. If the s_n -band states, such as the fourth or the sixth solutions, come into energetically lower positions in the higher angular momentum region, we can say that the band mixing [17] will become a key concept in understanding the band structure of the nucleus.

The last point is that we have found the new 3D-CHFB solutions along the prime meridian which have been obtained by the tilt-back calculation at $J = 18\hbar$ state. From the characteristic features of the solution, we can say that a new type of seesaw vibrational mode of the proton and the neutron pairing occurs in the back-bending region in ^{182}Os . This mode accompanies the large γ -oscillations. Thus a wobbling motion is expected to mediate a band crossing between the g -band and the s -band in this nucleus. The GCM calculation which includes these new solutions to explore the band structure of $A \sim 180$ mass region will be the next attractive subject.

Acknowledgments

The numerical calculations presented in the paper were

carried out by the Vector Parallel Processor, Fujitsu VPP500/28 at RIKEN. The authors would like to express their thanks to Dr. S.Yamaji and Dr. Y.Yano for kindly letting them use the facilities in the Nishina memorial building at RIKEN. One of us (AA) would like to thank the Japan Society for the Promotion of Science for financial support.

- [1] D.L. Hill and J.A. Wheeler, Phys. Rev. **89** (1953) 1102.
- [2] P. Chowdhury et al., Nucl. Phys. **A485** (1988) 136.
- [3] T.Horibata and N.Onishi, Phys. Lett. **B325** (1994) 283.
- [4] T.Horibata, M.Oi and N.Onishi, Phys. Lett. **B355** (1995) 433.
- [5] T.Horibata, M.Oi and N.Onishi, RIKEN Accel. Prog. Rep. **30** (1997) 20.
- [6] M.Oi, N.Onishi, N.Tajima and T.Horibata Phys. Lett. **B418** (1997) 1.
- [7] P. Bonche et al., Nucl. Phys. **A510** (1990) 466.
- [8] T.Horibata, M.Oi and N.Onishi, J. Phys. *to be published*.
- [9] T.Horibata and N.Onishi, Nucl. Phys. **A596** (1996) 251.
- [10] A.K. Kerman and N. Onishi, Nucl. Phys. **A361** (1981) 179, N. Onishi, Nucl. Phys. **A456** (1986) 279.
- [11] K. Hara, A. Hayashi and P. Ring, Nucl. Phys. **A385** (1982) 14, E.Wüst, A.Ansari and U.Mosel, Nucl. Phys. **A435** (1985) 477.
- [12] P.Ring and P.Schuck, *The Nuclear Many-Body Problem*, Springer-Verlag, Heidelberg, 1980.
- [13] C. Gustafson, I.L. Lamm, B. Nilsson and S.G. Nilsson, Arkiv. Fysik. **36** (1967) 613.
- [14] T. Horibata and N. Onishi, RIKEN Accel. Prog. Rep. **31** (1997) 22.
- [15] P.M.Walker et al., Phys. Lett. **B309** (1993) 17.
- [16] T.Kutsarova et al., Nucl. Phys. **A587** (1995) 111.
- [17] P.M.Walker, Proc. Future of Nuclear Spectroscopy, Crete (1993).